Check for updates

Probing enantioselectivity in rhodium-catalyzed Si–C bond cleavage to construct silicon-stereocenters: a theoretical study†

Zhaoyuan Yu, [iD] ‡[b] Tao Zhang,‡[b] Ruopeng Bai [iD] [b] and Yu Lan [iD] *[ab]

The rhodium-catalyzed asymmetric synthesis of dibenzooxasilines developed by Hayashi and co-workers provides an efficient method to construct tetraorganosilicon stereocenters. In the present study, density functional theory (DFT) calculations were performed to investigate the mechanism and enantioselectivity of this reaction. Theoretical calculations indicate that the mechanism involves the initial formation of an aryl-oxorhodium complex followed by Rh–Si exchange to afford an arylrhodium complex. The favorable oxidative addition/reductive elimination to cleave one Si–C(phenyl) bond from the arylrhodium complex determines the enantioselectivity. The enantioselectivity originates from the silyl moiety extruding from the phenyl ring on the rhodium atom in the reductive elimination transition state.
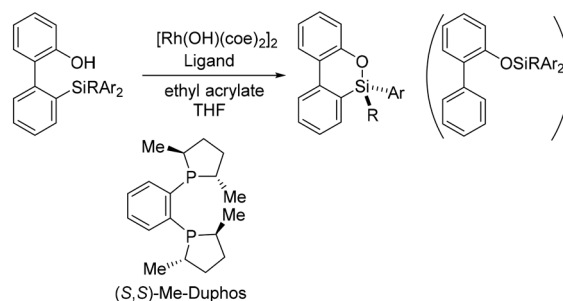
Introduction

Organosilicon compounds generally have high thermal and chemical stabilities and are readily available, relatively inexpensive and non-toxic; thus, as organometallic nucleophiles, they possess many advantages over other organometallic compounds.[1] Compared with other organometallic nucleophiles, organosilicon compounds are weak nucleophiles because the carbon-silicon bond is only weakly polarized.[2] Because of the above-mentioned special properties, organosilicon compounds are widely used in various transition-metal (*e.g.*, nickel,[3] copper,[4] iridium,[5] palladium,[6] rhodium,[7] ruthenium,[8] iron[9])-catalyzed organic reactions. For example, Chatani and co-workers reported rhodium-catalyzed intermolecular coupling of 2-trimethylsilylphenyl boronic acids with alkynes by the cleavage of an inactive C(sp³)–Si bond.[10] Xi and coworkers developed an efficient process involving Rh-catalyzed selective cleavage of a C(sp³)–Si bond and consequent *cis*-addition to a C–C unsaturated bond, affording silatricyclic compounds.[11] Murakami and coworkers presented a unique palladium-catalyzed intermolecular σ-bond exchange reaction between C–C and C–Si σ-bonds.[12]

Various methods are available for the preparation of carbon-stereogenic compounds.[13] In contrast, there are very limited reports on the synthesis of organosilicon compounds containing tetraorganosilicon stereocenters.[14] It is well known that chiral silicon compounds do not exist in nature. Therefore, broadening the scope of accessible chiral organosilicon compounds is highly desirable. The pioneering work on the asymmetric construction of chiral silicon centers was reported by the Corriu[15] and Kumada groups in the 1970s.[16] Since then, a number of catalytic systems have been developed for the synthesis of chiral silicon compounds.[17] For example, Nishihara and coworkers reported palladium-catalyzed enantioselective arylation of secondary silanes.[18] Takai and coworkers reported asymmetric rhodium-catalyzed Si–H silylation to synthesize spirosilabifluorene derivatives.[19]

Recently, Hayashi and coworkers reported a straightforward process for the formation of silicon-stereogenic organosilanes using rhodium-catalyzed enantioselective transmetallation of prochiral organosilicon compounds (Scheme 1).[20] A combination of [Rh(OH)(coe)₂]₂ and the (*S,S*)-Me-Duphos ligand afforded the product in 89% yield and 91% ee. However, the origin of the enantioselectivity was unclear. From the reaction shown in Scheme 1, formation of the chiral silicon center involves S–C bond cleavage. As we

[a] Department College of Chemistry and Molecular Engineering, Zhengzhou University, Zhengzhou, 450001, China. E-mail: lanyu@cqu.edu.cn
[b] School of Chemistry and Chemical Engineering, Chongqing University, Chongqing, 400030, China
† Electronic supplementary information (ESI) available. See DOI: 10.1039/c8cy02261e
‡ These authors contributed equally to this work.

Scheme 1 Rhodium-catalyzed asymmetric synthesis of dibenzooxasilines.

will see, how the Si–C bond is cleaved and how the cleavage is related to the formation of the chiral silicon center are especially interesting. In order to elucidate the key factors in the formation of the chiral silicon center, we carried out density functional theory (DFT) calculations to explore the reaction mechanisms and origins of the enantioselectivity of the reaction shown in Scheme 1.

Computational methods

All the DFT calculations were carried out with the GAUSSIAN 09 program package.[21] Density functional theory at the level of B3LYP[22] with the standard 6-31G(d) basis set[23] (LanL2DZ basis set[24] for rhodium atom) was used for geometry optimizations. Harmonic frequency calculations were performed at the same level of theory for all the stationary points to confirm them as local minima or transition structures and to derive the thermochemical corrections for the enthalpies and Gibbs free energies.

The recently developed MN12-L functional[25] was used to calculate the single point energies. Solvent (tetrahydrofuran) effects were also considered in the single point energy calculations based on the gas-phase optimized stationary points using the SMD solvation model.[26] The larger basis set 6-311+G(d,p) (LANL08f basis set[27] for the rhodium atom) was used in the single point energy calculations. The energies given and discussed in this paper are the solvation-corrected MN12-L calculated Gibbs free energies. The NCIPLOT analyses were conducted with Multiwfn[28] and VMD.[29] The 3D images of the calculated structures were prepared using CYLview.[30]

Results and discussion

From the reaction shown in Scheme 1, it is convenient to assume that the reaction mechanism involves O-coordination of a substrate molecule to Rh followed by oxidative addition (OA) involving Si–C bond cleavage and then reductive elimination to form an Si–O bond, affording the product molecule. In order to achieve this, two possible pathways must be considered.[31] Scheme 2 shows the two possible catalytic cycles. Both cycles start with A, a species generated from transmetallation between a monomeric Rh complex and the substrate. In path a (blue line), an Si–C(phenyl) bond is oxidatively added to the Rh(I) metal center of A to afford the Rh(III) intermediate B, which then undergoes Si–O bond-forming reductive elimination, producing the phenylrhodium species C and the dibenzooxasiline product. In path b, an alternative OA, which cleaves the Si–C(biphenyl) bond instead, occurs to afford a different Rh(III) intermediate (D), which undergoes Si–O bond-forming reductive elimination to provide E. The transformation of A to E is in fact achieved via a formal metathesis between the relevant Si–C and Rh–O bonds. From E, oxidative addition of one Si–C(phenyl) bond affords F, followed by reductive elimination, again yielding the phenylrhodium species C and the product. The two pathways
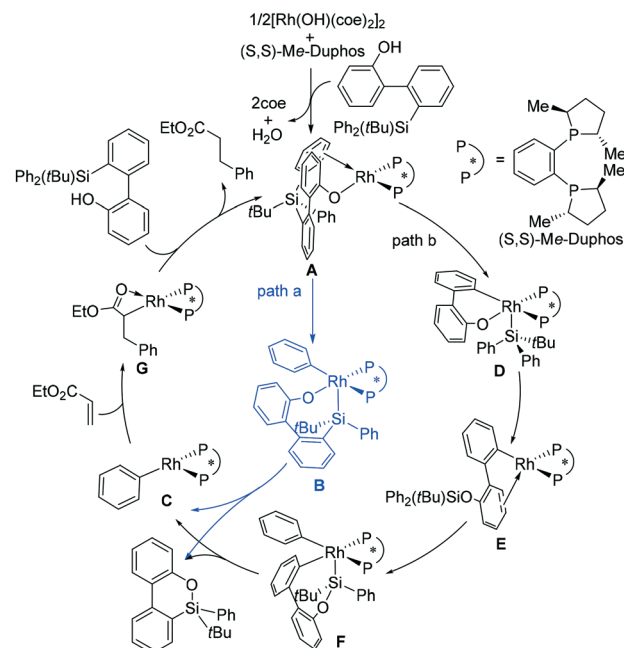
Scheme 2 Proposed mechanisms for the Rh-catalyzed synthesis of dibenzooxasilines.

join at the phenylrhodium species C. From C, insertion of ethyl acrylate into the Rh–phenyl bond takes place to afford the square-planar intermediate G, from which subsequent protonolysis with another substrate molecule regenerates the active aryloxorhodium species A and completes the catalytic cycle.

From Scheme 2, the active aryloxorhodium species A is formed by reacting the precatalyst with the substrate in the presence of the chiral ligand (S,S)-Me-Duphos. The formation of A from the precatalyst is indeed very thermodynamically favorable (see Fig. S1 in the ESI†), supporting the mechanistic hypothesis presented in Scheme 2.

Formation of the dibenzooxasiline from aryloxorhodium species A

On the basis of the mechanisms shown in Scheme 2, we first consider the oxidative addition (A → B) and reductive elimination (B → C) processes, as shown in Fig. 1. Experimentally, the (S,S)-Me-Duphos ligand affords the product in 89% yield and 91% ee; therefore, in our calculations, we used (S,S)-Me-Duphos as the ligand. Starting from active species A, in which one of the phenyl rings on the silicon atom coordinates with the Rh(I) center, intramolecular oxidative addition of the Si–C(phenyl) bond can take place via the transition state $TS_{A-B(R)}$ with a 21.2 kcal mol^{-1} barrier. The square pyramidal Rh(III) intermediate B-R is then formed and is endothermic by 15.3 kcal mol^{-1}. The subsequent reductive elimination occurs via the transition state $TS_{B-C(R)}$ with a free energy barrier of 7.2 kcal mol^{-1} relative to B-R and releases the (R)-configuration dibenzooxasiline product. Alternatively, the dibenzooxasiline product can be formed from complex A via a direct
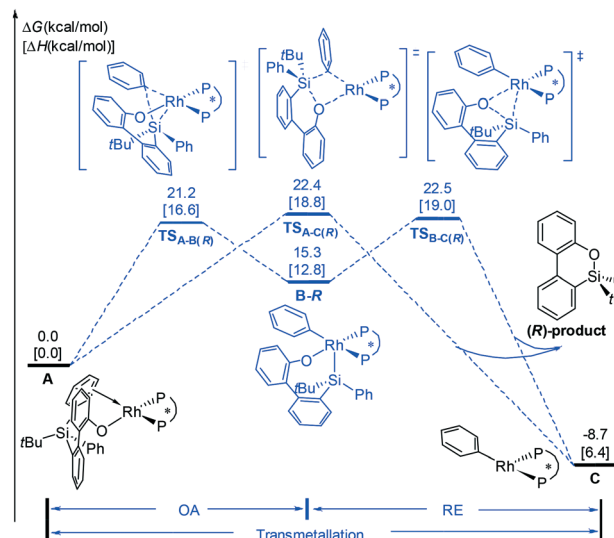
Fig. 1 The free energy profiles calculated for the formation of the (*R*)-configuration dibenzooxasiline product starting from intermediate **A**.

transmetallation transition state **TS$_{A-C(R)}$** with a 22.4 kcal mol^{-1} barrier.

Rh–Si exchange to form arylrhodium species E followed by transmetallation

According to previous experimental studies[32] and computational studies,[33] Rh–Si exchange may also occur. In the following sections, our main objective is to obtain deep insight into the cleavage of the Si–C(biphenyl) bond *versus* the Si–C(phenyl) bond. The calculated energy profiles to form arylrhodium complex **E** are shown in Fig. 2. The calculation results reveal that Si–C(biphenyl) bond cleavage *via* **TS$_{A-D}$** requires an activation free energy of 16.7 kcal mol^{-1} to afford the Rh(III) intermediate **D**. The generated intermediate **D** adopts a square pyramidal geometry and is endergonic by 3.0 kcal mol^{-1}. The subsequent reductive elimination process re-
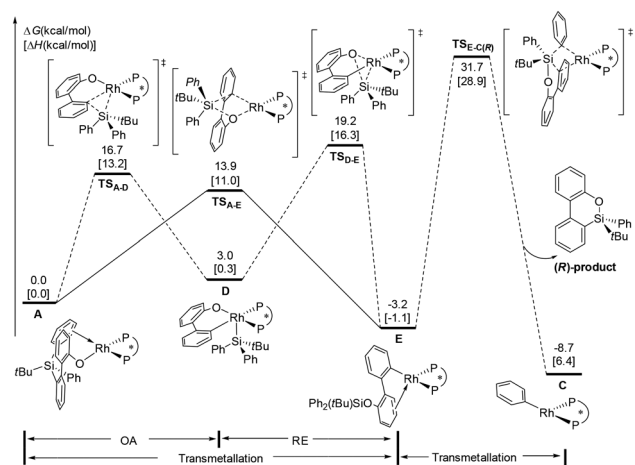
quires an overall barrier of 19.2 kcal mol^{-1} (from **A** to **TS$_{D-E}$**). On the other hand, the transmetallation pathway *via* transition state **TS$_{A-E}$** to afford the arylrhodium **E** is 5.3 kcal mol^{-1} lower in energy than the oxidative addition/reductive elimination pathway. The above results suggest that the Rh–Si exchange is an energy-downhill process and occurs directly *via* a transmetallation transition state.

From the π-coordinated arylrhodium complex **E** (Fig. 3), transmetallation of one of the two Si–C(phenyl) bonds *via* transition state **TS$_{E-C(R)}$** occurs to afford the (*R*)-configuration product and phenylrhodium complex **C** with a very high barrier of 34.9 kcal mol^{-1}. Clearly, this pathway is very energetically unfavorable. The energy profiles calculated for the formation of the byproduct from complex **E** are presented in the ESI† (Fig. S2).

Oxidative addition of the Si–C(phenyl) bond of arylrhodium species E

In addition to the transmetallation pathway, the alternative oxidative addition/reductive elimination pathway was explored. As shown in Fig. 4, a facile oxidative addition process can occur through transition state **TS$_{E-F(R)}$** to form intermediate **F-R**; subsequent reductive elimination affords the phenylrhodium **C** and the product. This stepwise pathway requires a 14.5 kcal mol^{-1} overall barrier from intermediate **E**. Therefore, our calculation results indicate that formation of the (*R*)-configuration product is favored *via* oxidative addition/reductive elimination of arylrhodium complex **E**, and reductive elimination of the Si–C(biphenyl) bond is the enantioselectivity-determining step.

The next issue that must be addressed is the origin of enantioselectivity. The free energy profile leading to the (*S*)-configuration product *via* the oxidative addition/reductive elimination pathway from arylrhodium complex **E** is illustrated in Fig. 4. The formation of the Rh(III) intermediate **F-S** *via* transition state **TS$_{E-F(S)}$** is slightly more favorable than that by **TS$_{E-F(R)}$**. However, the reductive elimination transition state **TS$_{F-C(S)}$** is 2.6 kcal mol^{-1} less stable than **TS$_{F-C(R)}$**. The above results suggest that oxidative addition/reductive

Fig. 2 The free energy profiles for Rh–Si exchange/transmetallation from intermediate **A**.

Fig. 3 Optimized structures of selected intermediates and transition states; distances are given in angstroms and angles in degrees.

648 | *Catal. Sci. Technol.*, 2019, **9**, 646–651

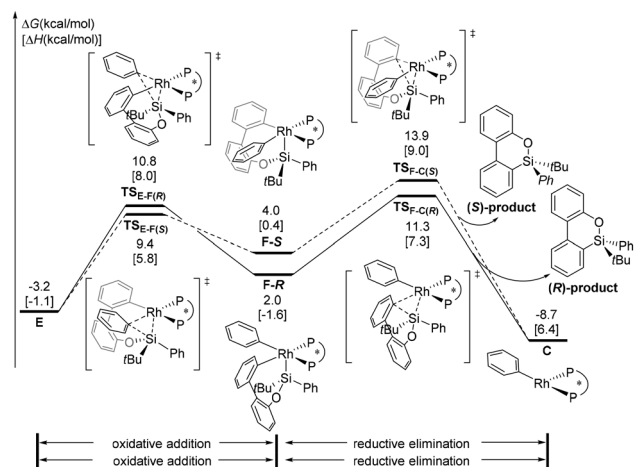This journal is © The Royal Society of Chemistry 2019

Fig. 4 The free energy profiles for the oxidative addition and reductive elimination mechanisms.

elimination leading to the observed (*R*)-configuration product is more favourable, and the value of ee (96%) predicted based on the energy difference between **TS$_{F-C(R)}$** and **TS$_{F-C(S)}$** is in good agreement with the experimental result (91%). From phenylrhodium **C**, the calculated energy profile to regenerate the active species complex **A** is given in the ESI† (Fig. S3).

In order to obtain details of the origins of the enantioselectivity of this reaction, all possible transition states that result in different chiral products were computed. The chiral environment created by the (*S,S*)-Me-Duphos ligand can be described according to the quadrant analysis (Fig. 5a).[34] The NE and SW quadrants are both occupied by methyl groups on the ligand; thus, these two quadrants are sterically more encumbered than the NW and SE quadrants (where the two hydrogen atoms are oriented toward the Rh center). These chiral pockets created by the ligand are expected to affect the orientations of the substrates. As shown in Fig. 5b, both **F-R** and **F-S** adopt square pyramidal geometries, and the silyl group occupies the vertex position. However, in the transition state **TS$_{F-C(R)}$**, the Si–C(biphenyl) bond forms in the SE quadrant (less steric repulsion quadrant). In contrast, in **TS$_{F-C(R)}$**, the Si–C(biphenyl) bond forms in the methyl group-blocked SW quadrant. Moreover, in the process of Si–C(biphenyl) bond formation, the silicon atom will approach the carbon atom of the Rh–C(biphenyl) bond accompanied by the silyl moiety, which tends to squeeze the phenyl ring (green phenyl group on the rhodium atom). In the structure of **TS$_{F-C(R)}$**, the dihedral angle of C1-Rh-P-C2 is 170.7°, which indicates that the phenyl ring on the rhodium is tilted slightly toward the NW quadrant. However, in the transition state **TS$_{F-C(S)}$**, the silyl group will extrude the phenyl group on the rhodium atom and tilt it toward the NE quadrant (methyl group-blocked quadrant). Consequently, the phenyl group is considerably distorted from the square-planar geometry to minimize steric interaction (the dihedral angle of C1-Rh-P-C2 in **TS$_{F-C(S)}$** is 109.6°).
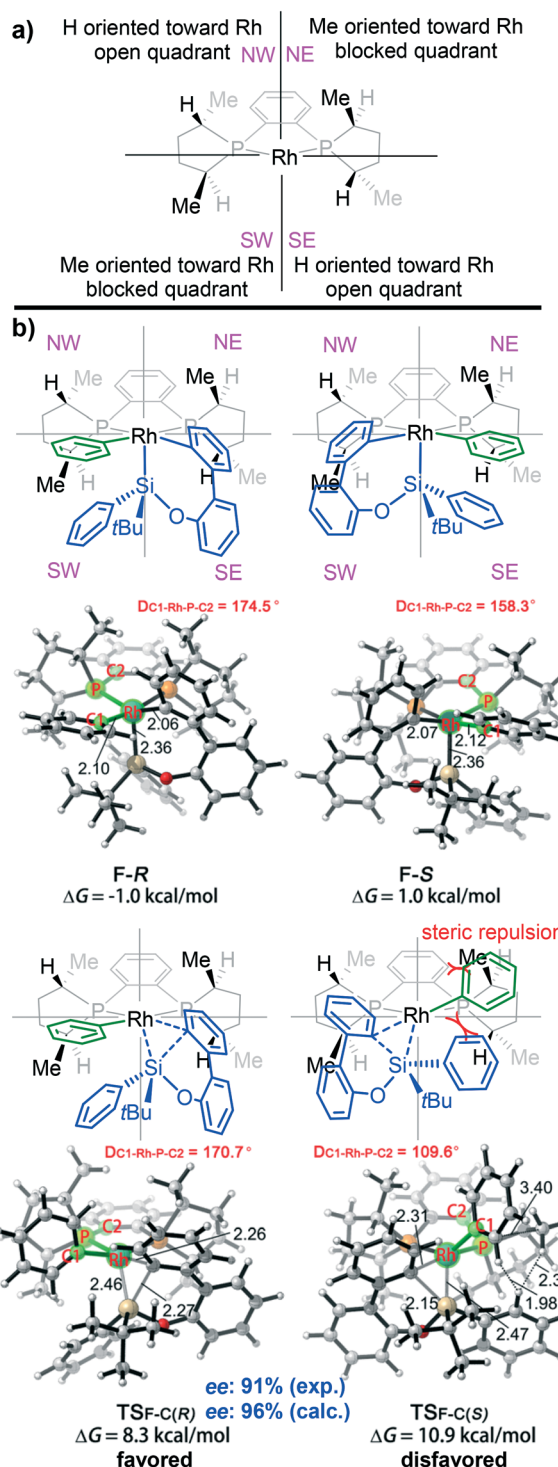

Fig. 5 (a) Quadrant analysis of the chiral environment created by the (*S,S*)-Me-Duphos ligand. (b) Optimized structures of **F-R**, **F-S**, **TS$_{F-C(R)}$** and **TS$_{F-C(S)}$**. Distances are given in angstroms and angles in degrees.

To obtain a clearer view of the steric repulsion induced by the spatial environment, NCIPLOT analysis was performed to describe the steric repulsion. As shown in Fig. 6, the higher activation energy barrier of transition state **TS$_{F-C(S)}$** can be rationalized by the labelled steric

This journal is © The Royal Society of Chemistry 2019

Catal. Sci. Technol., 2019, **9**, 646–651 | **649**

Fig. 6 NCIPLOTs of **TS**$_{F-C(R)}$ and **TS**$_{F-C(S)}$. The s = 0.6 au isosurface is colored according to a BGR scheme over the range of −0.02 < sign(λ_2)ρ < 0.02 au. Blue indicates strong attractions, green indicates very weak interactions, and red indicates strong repulsion.

repulsion between the phenyl groups on the silicon atom and the phosphine ligand.

Conclusions

In summary, the detailed mechanism of the rhodium-catalyzed asymmetric synthesis of dibenzooxasilines has been investigated with DFT calculations. The calculation results revealed that the mechanism consists of the following steps: (i) the hydroxorhodium complex initially undergoes deprotonation with the substrate to generate the aryloxorhodium intermediate; (ii) Rh–Si exchange occurs to afford the arylrhodium complex; (iii) oxidative addition/reductive elimination generates the dibenzooxasiline product; (iv) the active aryloxorhodium species **A** is regenerated with the aid of ethyl acrylate.

The related enantioselectivity of this reaction has also been investigated. The results indicate that the enantioselectivity is determined during the step of oxidative addition/reductive elimination from the arylrhodium complex. The origin of the enantioselectivity has been elucidated by quadrant analysis and NCIPLOT analysis. It was found that in the reductive elimination transition state **TS**$_{F-C(S)}$, the silyl group will squeeze the phenyl ring on the rhodium atom to tilt toward the methyl group-blocked quadrant, which causes significant steric repulsion and eventually leads to formation of the (*R*)-configuration product.

Conflicts of interest

There are no conflicts to declare.

Acknowledgements

References

1 (*a*) S. E. Denmark and C. S. Regens, *Acc. Chem. Res.*, 2008, **41**, 1486–1499; (*b*) S. E. Denmark and R. F. Sweis, *Acc. Chem. Res.*, 2002, **35**, 835–846; (*c*) T. Hiyama and E. Shirakawa, *Top. Curr. Chem.*, 2002, **219**, 61–85; (*d*) L. Li, Y. Zhang, L. Gao and Z. Song, *Tetrahedron Lett.*, 2015, **56**, 1466–1473.

2 (*a*) T. H. Chan and D. Wang, *Chem. Rev.*, 1992, **92**, 995–1006; (*b*) T. Komiyama, Y. Minami and T. Hiyama, *ACS Catal.*, 2017, **7**, 631–651; (*c*) Y. Nakao and T. Hiyama, *Chem. Soc. Rev.*, 2011, **40**, 4893–4901; (*d*) H. F. Sore, W. R. J. D. Galloway and D. R. Spring, *Chem. Soc. Rev.*, 2012, **41**, 1845–1866; (*e*) J. Sun and L. Deng, *ACS Catal.*, 2016, **6**, 290–300.

3 (*a*) K. Hirano, H. Yorimitsu and K. Oshima, *Org. Lett.*, 2006, **8**, 483–485; (*b*) K. Hirano, H. Yorimitsu and K. Oshima, *J. Am. Chem. Soc.*, 2007, **129**, 6094–6095; (*c*) J. Terao, H. Watabe, H. Watanabe and N. Kambe, *Adv. Synth. Catal.*, 2004, **346**, 1674–1678.

4 (*a*) S. K. Kang, T. H. Kim and S. J. Pyun, *J. Chem. Soc., Perkin Trans. 1*, 1997, **6**, 797–798; (*b*) Y. Nishihara, K. Ikegashira, K. Hirabayashi, J.-i. Ando, A. Mori and T. Hiyama, *J. Org. Chem.*, 2000, **65**, 1780–1787; (*c*) H. Taguchi, K. Ghoroku, M. Tadaki, A. Tsubouchi and T. Takeda, *J. Org. Chem.*, 2002, **67**, 8450–8456.

5 B. Su, T. G. Zhou, X. W. Li, X. R. Shao, P. L. Xu, W. L. Wu, J. F. Hartwig and Z. J. Shi, *Angew. Chem., Int. Ed.*, 2017, **56**, 1092–1096.

6 (*a*) Y. Hatanaka and T. Hiyama, *J. Org. Chem.*, 1988, **53**, 918–920; (*b*) Y. Hatanaka and T. Hiyama, *Tetrahedron Lett.*, 1990, **31**, 2719–2722; (*c*) K. Itami, T. Nokami and J.-i. Yoshida, *J. Am. Chem. Soc.*, 2001, **123**, 5600–5601; (*d*) Y. Liang, W. Geng, J. Wei and Z. Xi, *Angew. Chem., Int. Ed.*, 2012, **51**, 1934–1937; (*e*) Y. Liang, S. Zhang and Z. Xi, *J. Am. Chem. Soc.*, 2011, **133**, 9204–9207; (*f*) N. Miyaura, K. Yamada and A. Suzuki, *Tetrahedron Lett.*, 1979, **20**, 3437–3440; (*g*) J.-i. Yoshida, K. Tamao, M. Takahashi and M. Kumada, *Tetrahedron Lett.*, 1978, **19**, 2161–2164.

7 (*a*) T.-S. Huang and C.-J. Li, *Chem. Commun.*, 2001, 2348–2349; (*b*) T. Matsuda and Y. Ichioka, *Org. Biomol. Chem.*, 2012, **10**, 3175–3177; (*c*) C. Walter and M. Oestreich, *Angew. Chem., Int. Ed.*, 2008, **47**, 3818–3820; (*d*) M. Yu and X. Fu, *J. Am. Chem. Soc.*, 2011, **133**, 15926–15929; (*e*) Q. W. Zhang, K. An and W. He, *Angew. Chem., Int. Ed.*, 2014, **53**, 5667–5671.

8 F. Delpech, J. Mansas, H. Leuser, S. Sabo-Etienne and B. Chaudret, *Organometallics*, 2000, **19**, 5750–5757.

9 (*a*) H. Hashimoto, A. Matsuda and H. Tobita, *Organometallics*, 2006, **25**, 472–476; (*b*) H. Nakazawa, K. Kamata and M. Itazaki, *Chem. Commun.*, 2005, 4004–4006; (*c*) E. Shirakawa, S. Masui, R. Narui, R. Watabe, D. Ikeda and T. Hayashi, *Chem. Commun.*, 2011, **47**, 9714–9716.

10 M. Onoe, K. Baba, Y. Kim, Y. Kita, M. Tobisu and N. Chatani, *J. Am. Chem. Soc.*, 2012, **134**, 19477–19488.

11 Q. Yang, L. Liu, Y. Chi, W. Hao, W.-X. Zhang and Z. Xi, *Org. Chem. Front.*, 2018, **5**, 860–863.

12 S. Okumura, F. Sun, N. Ishida and M. Murakami, *J. Am. Chem. Soc.*, 2017, **139**, 12414–12417.

13 (*a*) X. Chen, K. M. Engle, D. H. Wang and J. Q. Yu, *Angew. Chem., Int. Ed.*, 2009, **48**, 5094–5115; (*b*) J. Hassan, M. Sévignon, C. Gozzi, E. Schulz and M. Lemaire, *Chem. Rev.*, 2002, **102**, 1359–1470; (*c*) N. Miyaura and A. Suzuki, *Chem. Rev.*, 1995, **95**, 2457–2483; (*d*) E. Negishi, *Acc. Chem. Res.*, 2002, **15**, 340–348; (*e*) A. Suzuki, *J. Organomet. Chem.*, 1999, **576**, 147–168; (*f*) A. Suzuki, *Acc. Chem. Res.*, 2002, **15**, 178–184.

14 (*a*) X. F. Bai, J. F. Zou, M. Y. Chen, Z. Xu, L. Li, Y. M. Cui, Z. J. Zheng and L. W. Xu, *Chem. - Asian J.*, 2017, **12**, 1730–1735; (*b*) J. O. Bauer and C. Strohmann, *Angew. Chem., Int. Ed.*, 2014, **53**, 720–724; (*c*) J. O. Bauer and C. Strohmann, *Eur. J. Inorg. Chem.*, 2016, **2016**, 2868–2881; (*d*) K. Igawa, D. Yoshihiro, Y. Abe and K. Tomooka, *Angew. Chem., Int. Ed.*, 2016, **55**, 5814–5818; (*e*) P.-W. Long, X.-F. Bai, F. Ye, L. Li, Z. Xu, K.-F. Yang, Y.-M. Cui, Z.-J. Zheng and L.-W. Xu, *Adv. Synth. Catal.*, 2018, **360**, 2825–2830; (*f*) R. Shintani, *Asian J. Org. Chem.*, 2015, **4**, 510–514; (*g*) R. Shintani, C. Takagi, T. Ito, M. Naito and K. Nozaki, *Angew. Chem., Int. Ed.*, 2015, **54**, 1616–1620; (*h*) H. Wen, X. Wan and Z. Huang, *Angew. Chem., Int. Ed.*, 2018, **57**, 6319–6323; (*i*) G. Zhan, H. L. Teng, Y. Luo, S. J. Lou, M. Nishiura and Z. Hou, *Angew. Chem., Int. Ed.*, 2018, **57**, 12342–12346; (*j*) Q.-W. Zhang, K. An, L.-C. Liu, Q. Zhang, H. Guo and W. He, *Angew. Chem., Int. Ed.*, 2017, **56**, 1125–1129; (*k*) W.-T. Zhao, Z.-Q. Lu, H. Zheng, X.-S. Xue and D. Zhao, *ACS Catal.*, 2018, **8**, 7997–8005.

15 (*a*) R. J. P. Corriu and J. J. E. Moreau, *J. Organomet. Chem.*, 1974, **64**, C51–C54; (*b*) R. J. P. Corriu and J. J. E. Moreau, *Tetrahedron Lett.*, 1973, **14**, 4469–4472.

16 T. Hayashi, K. Yamamoto and M. Kumada, *Tetrahedron Lett.*, 1974, **15**, 331–334.

17 (*a*) R. Shintani, K. Moriya and T. Hayashi, *J. Am. Chem. Soc.*, 2011, **133**, 16440–16443; (*b*) R. Shintani, H. Otomo, K. Ota and T. Hayashi, *J. Am. Chem. Soc.*, 2012, **134**, 7305–7308; (*c*) R. Shintani, R. Takano and K. Nozaki, *Chem. Sci.*, 2016, 7, 1205–1211.

18 Y. Kurihara, M. Nishikawa, Y. Yamanoi and H. Nishihara, *Chem. Commun.*, 2012, **48**, 11564–11566.

19 (*a*) Y. Kuninobu, K. Yamauchi, N. Tamura, T. Seiki and K. Takai, *Angew. Chem., Int. Ed.*, 2013, **52**, 1520–1522; (*b*) M. Murai, Y. Takeuchi, K. Yamauchi, Y. Kuninobu and K. Takai, *Chem. - Eur. J.*, 2016, **22**, 6048–6058.

20 R. Shintani, E. E. Maciver, F. Tamakuni and T. Hayashi, *J. Am. Chem. Soc.*, 2012, **134**, 16955–16958.

21 M. J. T. Frisch, G. W. Trucks, H. B. Schlegel, G. E. Scuseria, M. A. Robb, J. R. Cheeseman, G. Scalmani, V. Barone, B. Mennucci, G. A. Petersson, H. Nakatsuji, M. Caricato, X. Li, H. P. Hratchian, A. F. Izmaylov, J. Bloino, G. Zheng, J. L. Sonnenberg, M. Hada, M. Ehara, K. Toyota, R. Fukuda, J. Hasegawa, M. Ishida, T. Nakajima, Y. Honda, O. Kitao, H. Nakai, T. Vreven, J. A. Montgomery Jr., J. E. Peralta, F. Ogliaro, M. Bearpark, J. J. Heyd, E. Brothers, K. N. Kudin, V. N. Staroverov, R. Kobayashi, J. Normand, K. Raghavachari, A. Rendell, J. C. Burant, S. S. Iyengar, J. Tomasi, M. Cossi, N. Rega, J. M. Millam, M. Klene, J. E. Knox, J. B. Cross, V. Bakken, C. Adamo, J. Jaramillo, R. Gomperts, R. E. Stratmann, O. Yazyev, A. J. Austin, R. Cammi, C. Pomelli, J. W. Ochterski, R. L. Martin, K. Morokuma, V. G. Zakrzewski, G. A. Voth, P. Salvador, J. J. Dannenberg, S. Dapprich, A. D. Daniels, O. Farkas, J. B. Foresman, J. V. Ortiz, J. Cioslowski and D. J. Fox, *Gaussian 09*, Revision D.01, Gaussian, Inc., Wallingford, CT, 2013.

22 (*a*) A. D. Becke, *J. Chem. Phys.*, 1993, **98**, 5648–5652; (*b*) C. Lee, W. Yang and R. G. Parr, *Phys. Rev. B*, 1988, **37**, 785–789; (*c*) P. J. Stephens, F. J. Devlin, C. F. Chabalowski and M. J. Frisch, *J. Phys. Chem.*, 1994, **98**, 11623–11627.

23 (*a*) J. D. Dill and J. A. Pople, *J. Chem. Phys.*, 1975, **62**, 2921–2923; (*b*) M. M. Francl, W. J. Pietro, W. J. Hehre, J. S. Binkley, M. S. Gordon, D. J. DeFrees and J. A. Pople, *J. Chem. Phys.*, 1982, **77**, 3654–3665; (*c*) W. J. Hehre, R. Ditchfield and J. A. Pople, *J. Chem. Phys.*, 1972, **56**, 2257–2261.

24 (*a*) P. J. Hay and W. R. Wadt, *J. Chem. Phys.*, 1985, **82**, 270–283; (*b*) P. J. Hay and W. R. Wadt, *J. Chem. Phys.*, 1985, **82**, 299–310; (*c*) W. R. Wadt and P. J. Hay, *J. Chem. Phys.*, 1985, **82**, 284–298.

25 R. Peverati and D. G. Truhlar, *Phys. Chem. Chem. Phys.*, 2012, **14**, 13171–13174.

26 (*a*) A. V. Marenich, C. J. Cramer and D. G. Truhlar, *J. Phys. Chem. B*, 2009, **113**, 6378–6396; (*b*) A. V. Marenich, C. J. Cramer and D. G. Truhlar, *J. Phys. Chem. B*, 2009, **113**, 4538–4543.

27 (*a*) A. W. Ehlers, M. Böhme, S. Dapprich, A. Gobbi, A. Höllwarth, V. Jonas, K. F. Köhler, R. Stegmann, A. Veldkamp and G. Frenking, *Chem. Phys. Lett.*, 1993, **208**, 111–114; (*b*) L. E. Roy, P. J. Hay and R. L. Martin, *J. Chem. Theory Comput.*, 2008, **4**, 1029–1031; (*c*) Z. Yu, Z. Jin, M. Duan, R. Bai, Y. Lu and Y. Lan, *J. Org. Chem.*, 2018, **83**, 9729–9740.

28 (*a*) E. R. Johnson, S. Keinan, P. Mori-Sanchez, J. Contreras-Garcia, A. J. Cohen and W. Yang, *J. Am. Chem. Soc.*, 2010, **132**, 6498–6506; (*b*) T. Lu and F. Chen, *J. Comput. Chem.*, 2012, **33**, 580–592.

29 W. Humphrey, A. Dalke and K. Schulten, *J. Mol. Graphics*, 1996, **14**, 33–38.

30 C. Y. Legault, *CYLview, 1.0b*, Université de Sherbrooke, 2009, (http://www.cylview.org).

31 (*a*) W. J. Chen and Z. Lin, *Dalton Trans.*, 2014, **43**, 11138–11144; (*b*) H. Xie, H. Zhang and Z. Lin, *New J. Chem.*, 2013, **37**, 2856; (*c*) J. Zhang, J. Z. Xu, Z. J. Zheng, Z. Xu, Y. M. Cui, J. Cao and L. W. Xu, *Chem. - Asian J.*, 2016, **11**, 2867–2875; (*d*) T. Zhou, L. Xu and Y. Xia, *Org. Lett.*, 2013, **15**, 6074–6077; (*e*) T. Zhou and Y. Xia, *Organometallics*, 2014, **33**, 4230–4239.

32 T. Seiser and N. Cramer, *Angew. Chem., Int. Ed.*, 2010, **49**, 10163–10167.

33 Z. Yu and Y. Lan, *J. Org. Chem.*, 2013, **78**, 11501–11507.

34 (*a*) S. E. Denmark, W. T. Chang, K. N. Houk and P. Liu, *J. Org. Chem.*, 2015, **80**, 313–366; (*b*) C. Zheng, C. X. Zhuo and S. L. You, *J. Am. Chem. Soc.*, 2014, **136**, 16251–16259.

This journal is © The Royal Society of Chemistry 2019

Catal. Sci. Technol., 2019, **9**, 646–651 | **651**